Ultrafast Studies of Imaging Processes

Sabrina J. Diol

Center for Photoinduced Charge Transfer, Department of Chemistry, University of Rochester, Rochester, New York 14627

R. J. Dwayne Miller‡

Departments of Chemistry and Physics, University of Toronto, Toronto, Ontario, M5S-1A1, Canada

Interfacial electron transfer is the most fundamental process driving all imaging technologies. The advent of ultrafast lasers has led to the development of novel experimental techniques to probe such dynamics. This article presents five time domain spectroscopies that allow direct measurement of different segments of the electron trajectory across a heterogeneous interface. Electro-optic sampling measures field-assisted transport of carriers to the surface. Time-resolved two-photon photoemission enables measurement of electron relaxation at surfaces. Time-correlated single-photon counting, transient grating, and transient absorption techniques are implemented to determine electron transfer rates at interfaces. With these real-time approaches, the primary photophysical and photochemical processes at semiconductor/liquid interfaces and dye-sensitized semiconductors can be studied directly. The new information forthcoming from such studies is that electron transfer processes can be extremely fast at surfaces, in a range approaching adiabatic coupling conditions between the delocalized bond states and discrete molecular donor or acceptor states. This observation leads to a new conceptual framework for understanding photoinduced interfacial charge transfer processes.

Journal of Imaging Science and Technology 41: 99–111 (1997)

Introduction

Charge transfer and separation across an interface is the fundamental process behind essentially all light-based imaging technologies.[1–4] For example, the primary step behind the photographic process involves electron transfer from a dye into the conduction band of silver halides. The subsequent electron trapping and formation of reduced silver grains ultimately leads to the photographic latent image, however, the initial event triggering the process is the interfacial electron transfer. The xerographic process similarly involves a charging step. In this case, charge transfer involves mass transfer as well (tribocharging). Even electronic imaging, using CCDs for spatial resolution, involves interfacial charge transfer across a solid state junction and charge storage. In addition to imaging technologies, interfacial charge transfer forms the basis for the entire field of electrochemistry.[5–6]

Original manuscript received August 15, 1996.

‡ To whom correspondence may be sent.

Given the technological and fundamental importance of this reaction process, considerable effort, spanning several decades, has been directed toward understanding this process.[4,7–11] Despite these efforts from various research communities, a detailed understanding of heterogeneous charge transfer between a conducting surface and a discrete molecular state is incomplete.[4] Here we primarily refer to solid/molecular (acceptor or donor) interfaces. For all solid state junctions, the purely electronic nature of interfacial charge transfer reduces the level of detail needed to understand the problem. There are three fundamental issues that need to be understood or determined in order to control heterogeneous electron transfer:

1. The relative energetics of the coupled state are not well defined.
2. The degree of electronic coupling or wave function overlap between electronic levels and molecular state was not known, even at a qualitative level, until just recently.
3. The relaxation process in both the solid state and molecular half space of the interface, which localize the charge, are only understood at a qualitative level and are usually extrapolated from bulk studies.

In contrast to heterogeneous electron transfer, these three primary processes (energetics, electronic coupling, and relaxation or barrier crossing dynamics) are becoming fairly well understood at a first principle level for the analogous problem of electron transfer between molecular acceptors and donors in solution (homogeneous electron transfer). The discrepancy in the level of understanding between heterogeneous and homogeneous electron transfer is simply due to the inherent greater difficulties in studying interfaces relative to solutions. To be specific, the most significant advances in understanding intermolecular electron transfer have come from combining dynamical measurements with different molecular acceptor/donor probes of the electron transfer coordinate. Studies along these lines most often exploit photoinduced electron transfer and short laser pulses to resolve the dynamics fully. In this regard, the photoinduced electron transfer process that serves as the basis of imaging technologies should be well suited to similar probes of heterogeneous electron transfer. However, in solution studies, it is possible to arrange the experimental conditions to probe 10^{16} reactive states/cm^2 within a given volume element to yield large changes in optical absorption due to either the formation of reactants or the disappearance of products. For weakly absorbing probe transitions, the concentration can generally be increased to give adequate signal to noise. For interfacial studies of charge transfer, the number of reactive states probed must be of the order of 10^{12}/cm^2 or

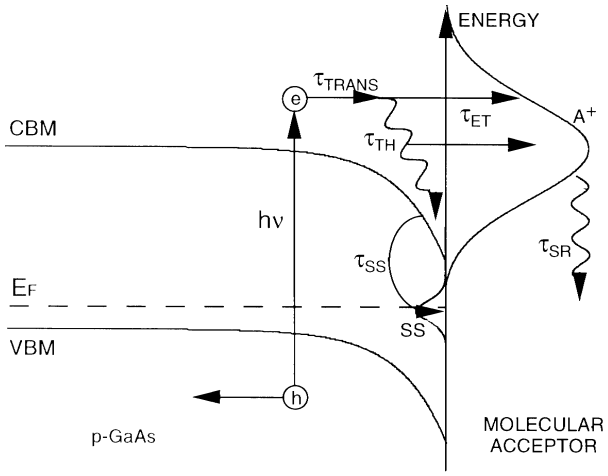

Figure 1. Photophysics at the semiconductor/electrolyte junction relevant to interfacial electron transfer, i.e., electron emission. Pathways for the competing dynamics of electron transport, thermalization, transfer, and trapping are shown and defined in the text. SR represents solvent reorganization, SS denotes surface states, and the curve labeled A^+ is the molecular electron acceptor distribution at the surface. The values *CBM*, *VBM*, and E_F represent the conduction band, valence band, and Fermi level, respectively.

less to avoid Coulombic effects (space charge effects) from complicating the kinetics. Even for complete monolayer coverage and neglecting Coulombic considerations, the maximum number of states that can be probed is on the order of $10^{13}/cm^2$ (for molecules with unit oscillator strength). Thus, spectroscopic approaches designed to probe interfacial charge transfer at well-defined crystal interfaces must be 10^3 to 10^4 more sensitive than conventional approaches used for bulk studies. In addition, the method must be surface selective; otherwise bulk signals will dominate any photoinduced response.

This high degree of sensitivity and surface selectivity has remained a great challenge for experimentalists. Only in the past few years, with sufficient progress in spectroscopic methods and laser technology, has exploring this domain been possible.[12,13] This article reviews the recent progress in this area with the objective of achieving a real-time view of the photoinduced and photochemical processes behind imaging.

Initial Boundary Conditions

One of the advantages of using optical time domain methods to study interfacial charge transfer is that one can optically prepare the system with two distinct $t = 0$ boundary conditions. A short excitation pulse prepares a nonequilibrium distribution of electrons at or near the surface reaction plane. The wavelength of the excitation pulse can be tuned to prepare the system in which the reactive, nonequilibrium, electronic states are localized either in the solid state or on the molecular half space of the interface. In the case the reactive charge carrier is initially localized in the solid state, the charge transfer process will be referred to as the **emission case**, i.e., the charge is leaving the solid state. For the opposite $t = 0$ boundary condition in which the reactive state is localized on the molecular acceptor or donor at the interface, the charge transfer process will be referred to as **electron injection**, i.e., the charge is injected into the solid state. The latter $t = 0$ boundary condition is only possible to achieve with wide bandgap semiconductors and is exactly the photographic process of dye sensitization.

The photophysics of electron transfer or electron emission at a semiconductor electrolyte junction are depicted in Fig. 1. The initial step is the optical preparation of an excited carrier distribution within the semiconductor. This preparation is accomplished using strongly absorbed above-bandgap light tuned to a high density of states direct transition such that a large fraction of the photocarriers are generated within the space-charge region. The case for a *p*-type junction is shown. The space-charge field accelerates the minority carriers, in this case, electrons, to the surface (τ_{TRANS}) while the holes are driven into the bulk. The carriers thermalize via various scattering mechanisms (τ_{TH}), and when a molecular acceptor with favorable energetics is present at the surface, the electrons undergo interfacial charge transfer (τ_{ET}). In the absence of any relaxation process, the electron would simply sample the distribution of molecular acceptors (denoted by the Gaussian distribution of A^+ in Fig. 1) and only have a brief residence time on any molecular acceptor. Nuclear fluctuations (solvent/intramolecular) that stabilize the charge on the molecular state drive the two coupled electronic states apart and localize the electron on the molecular acceptor. For a liquid interface, this nuclear relaxation process is usually dominated by solvent motion and is depicted by τ_{SR}. In competition with this direct electron-transfer process is the trapping of electrons within surface defects (τ_{SS}) that create localized states within the bandgap. Electron transfer to molecular states can also proceed through those surface state intermediates. As seen from this figure, at least five photophysical processes occur that dynamically control the path for interfacial electron transfer. Conventional electrochemical approaches give information on the energetics and quantum yields but are incapable of extracting the information necessary to understand the primary processes controlling the electron transfer. Various experimental methods have been developed capable of directly monitoring the different photophysical processes that when taken together give a real-time view of the electron-transfer transition-state region. For these studies GaAs (100) was selected as a model system because it has well-characterized optical, electronic, and electrochemical properties.[14]

Figure 2 illustrates the complementary process of electron injection from a molecular system to a semiconductor at a dye-sensitized semiconductor surface. The initial step is the photogeneration of the excited dye state to prepare a molecular state near resonance with conduction band states. A significant fraction of the excited electron population is transferred or injected (τ_{ET}) into the semiconductor followed by carrier thermalization and subsequent trapping by defects (τ_{SS}). Back electron transfer to the parent cation is also shown as geminate recombination (τ_{GR}), however nongeminate recombination involving electrons from other states can also occur. The overall quantum yield for sensitization (or photoanodic current) depends on the branching ratios between charge separation and these back transfer processes. As with the photoemission case, a number of distinct photophysical processes occur that control the electron transfer process. Many of these processes occur on femtosecond time scales and require ultrafast optical methods to study. Dye-sensitized SnS_2 was chosen as an ideal surface to probe these dynamics. SnS_2 is one of the few materials exhibiting high quantum yields (> 80%) for electron collection efficiency.[15,16] The material is a chemically inert, layered, two-dimensional semiconductor with optical properties suitable to a variety of experimental techniques. Ideally, one would like to study these dynamics at silver halide surfaces but the very photochemistry responsible for the

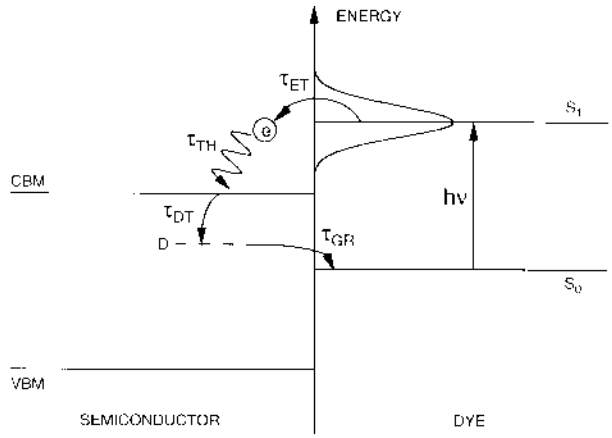

Figure 2. Photoinduced charge injection at a dye-sensitized semiconductor interface. Absorption of a photon prepares the system in the first excited singlet state (S_1) of the dye. The excited-state electrons are then injected into the semiconductor (τ_{ET}). The ensuing dynamics of thermalization (τ_{TH}), defect state trapping (τ_{DT}), and back electron transfer or geminate recombination (τ_{GR}) are also shown. CBM, VBM, and D represent the conduction band minimum, valence band maximum, and defect state level, respectively. The case depicted here is the optimal one in which the excited state lies above the conduction band. These energetics represent the barrierless case for interfacial electron transfer. In cases where the first excited state lies below the CBM, the electron dynamics become dominated by the nuclear activation barrier and one cannot extract information on the primary processes and electronic factors. The case depicted gives the fastest electron transfer dynamics for a given interface.

photographic process prevents repetitive sampling required by optical time-domain studies. The solution to this problem is to conduct experiments at low temperatures (< 120 K) to avoid photodecomposition.

Electron Emission

Field Transport: Electro-Optic Sampling of Surface Fields. A semiconductor in contact with a redox solution redistributes charge until the Fermi level of the semiconductor is equal to the solution redox potential (or solution Fermi level). This equilibration of the Fermi potential across the interface leads to the formation of a junction (liquid junction) in close analogy to a semiconductor/metal Shottky junction.[17] The space-charge region that develops in the semiconductor regions (depicted by the curved bands in Fig. 1) represents an enormous electric field (10^6 V/cm to 10^5 V/cm depending on the doping level) that serves to separate the photogenerated electron–hole pairs and drives the minority carriers to the surface reaction plane. For *p*-type materials, the electron is driven to the surface, whereas for *n*-type it is the hole. During the transit time across the space-charge region, the minority carrier is field accelerated and gains momentum (as illustrated by the straight line in relation to the curved band in Fig. 1). In the absence of thermalization, the carriers pick up approximately 1 eV of excess energy and arrive at the surface hot. The field acceleration determines the initial energetics of the carrier distribution at the surface and can be characterized by studies of carrier thermalization (below). In addition to the above consideration, the transit time of the carriers across the interface determines the upper limit of the time resolution to the interfacial charge-transfer dynamics. To completely resolve all the relevant dynamics, the carrier arrival time into the surface reaction plane should be shorter than the other dynamics of interest and needs to be convolved with the other dynamical variables. The problem is how to resolve the electron transport to the surface. This process is expected to be extremely fast and involves field-accelerated motion of only a few hundred angstroms for typical space-charge widths.

A new technique was developed based on electro-optic sampling. The basic idea behind this experiment is that the carrier separation and field-assisted transport leads to field amplitude changes in the space-charge region.[18–21] This point can be seen by considering Poisson's equation for the change in electric field, $\Delta E(x,t)$, i.e.,

$$\Delta E(x,t) = E_{SC} - \left(\frac{e}{4\pi\varepsilon\varepsilon_0}\right)\int_{-\infty}^{0}\big(p(x,t) - n(x,t)\big)dx,$$

where E_{SC} is the built in space charge field, e is the fundamental unit of charge, ε is the material dielectric constant, ε_0 is the permittivity of vacuum, $n(x,t)$ is the electron carrier density, $p(x,t)$ is the hole density, and x refers to the direction along the surface normal with $x = 0$ defining the surface position. At $t = 0$, the electron and hole distributions overlap ($n(x,t) = p(x,t)$) and no change in the field occurs. However, later the carrier distributions separate and a change in field amplitude develops. These field changes are directly related to the carrier transport and can be followed through the electro-optic effect. To use the electro-optic effect, the crystal must lack a center of symmetry and have some partial ionic character to the lattice bonding. These properties make the crystal electro-optic and are found in a rather large class of compounds including the III-V and II-VI semiconductors. With these properties, the electric field changes couple to the lattice and lead to the displacement of polar optical and acoustic lattice modes that in turn lead to induced birefringence. In essence, as the charge separates, a lattice distortion accompanies the change in charge distribution. By using polarization-sensitive probes, the carrier transport to the surface can be monitored directly.

The electro-optic method was developed for the analysis of high-speed solid state devices where conventional electronics do not have enough electrical bandwidth.[18] Typically, an electro-optic crystal is placed in the circuit in a traveling wave configuration or an evanescent field probe is used. In either case, the time resolution is limited by velocity mismatches between the propagation of the electric field and the probe pulse. By optically injecting charge in the space-charge region and monitoring the field changes directly where they occur, it was possible to avoid geometrical constraints on the time resolution. Thus, the fundamental upper limit to the time resolution for monitoring electric field transients was attained.[21] For GaAs (100), this resolution limit is approximately 30 fs (30×10^{-15} s) or 8-THz electrical bandwidth, which is determined by the highest frequency optical phonon. This time resolution is sufficient to follow ballistic electron motion over 100-Å-length scales, and applications in studying ballistic electron devices may be possible in the future. This general approach has also been used to study the phonons[22a] themselves and more recently to excite surface phonons.[22b]

The general features of the experiment are shown schematically in Fig. 3 in which the charge distributions are correlated to the electro-optic-induced index of refraction changes. The experimental setup is illustrated in Fig. 4. Experimental details can be obtained elsewhere.[20,21] Representative data are shown in Fig. 5 in which a *n*-GaAs (100)/oxide junction was studied as a model system. The rise time in the electric field, as monitored in reflection in a pump–probe configuration, shows a 200-fs rise time for

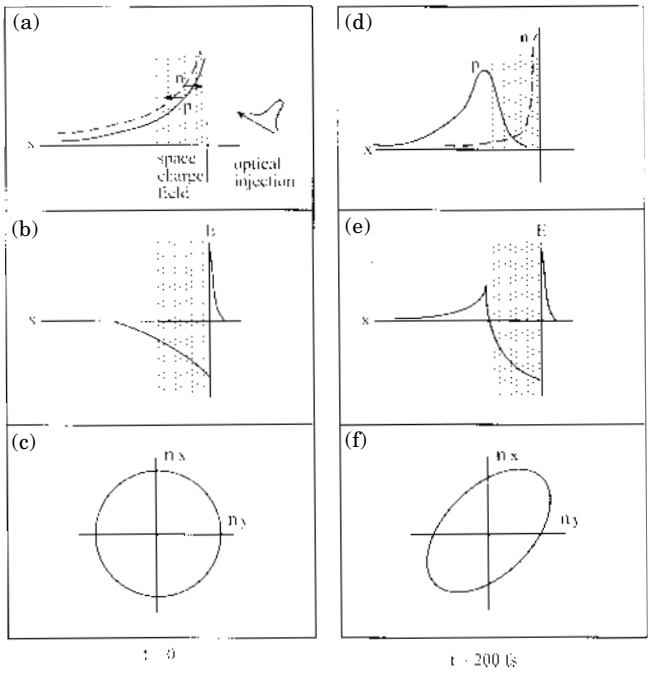

Figure 3. Schematic for electro-optic sampling. Figures 3 (a) through 3(c) and Figs. 3(e) through 3(f) represent changes in the sample at $t = 0$ and 200 fs after optical excitation, respectively. The space-charge region is designated by the dotted area at the sample surface. (a) and (d) the distribution of electrons and holes, (b) and (e) associated electric fields, and (c) and (f) electro-optic-induced change in the index of refraction are illustrated. The transport of minority carriers to the surface can be studied directly by using polarization-sensitive probes to monitor the electro-optic-induced birefringence.

photocarrier injection conditions of 3×10^{17} cm^{-3} (or 3×10^{12} photons/cm^2). Because the charge displacement changes the space-charge field, the carrier transport and arrival statistics of the minority carriers at the surface depend on the level of injection. This problem was analyzed in detail using an ensemble Monte Carlo approach with a Poisson equation solver to simulate the field dynamics and calculate the corresponding carrier distribution.[23-25] These results are shown in Fig. 6. The experimental results are in good agreement with the simulation. Interestingly enough, only one fast dynamical component was observed both experimentally and in the simulations (at these excitation levels). The most simple picture of the carrier transport would be field-accelerated transport across the space-charge region followed by a slower diffusive component for those carriers generated spatially outside the field region. By analysis of the simulation results, the separation of charge was found to create a transient field that acts as a Coulombic barrier to diffusion of the minority carriers from outside the space-charge region toward the surface. At injection levels of $> 10^{11}$/cm^2, this barrier is larger than kT and only one component is observed. At lower injection one observes the diffusive component, i.e., the transport to the surface is actually slower (involves both field-assisted and diffusive transport). At higher injection one observes only the field-assisted transport component of the carriers initially generated within the space-charge region. This is an important result as these conditions are the same as those used in the electron-transfer studies (surface grating studies, described below) and defines an operational time resolution to the ensuing interfacial charge transfer of approximately 100 fs. This time resolution is fast enough to time resolve all the relevant dynamics and for the first time enables

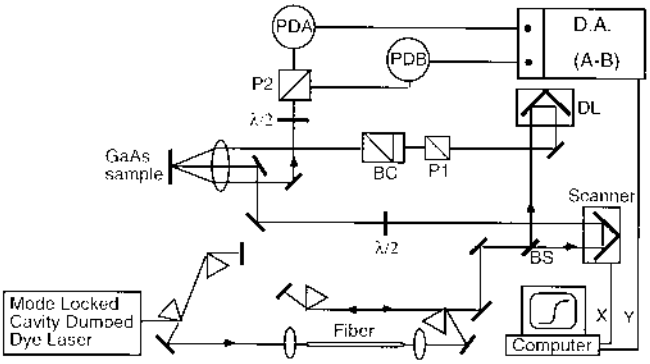

Figure 4. Reflective electro-optic sampling experimental setup. BS = beamsplitter, Scanner = PZT rapid scanner, λ/2 = halfwave plate, P1 and P2 = polarizers, BC = Babinet compensator, PDA and PDB = photodiodes, D.A. = differential amplifier, and computer = computer averaging system.

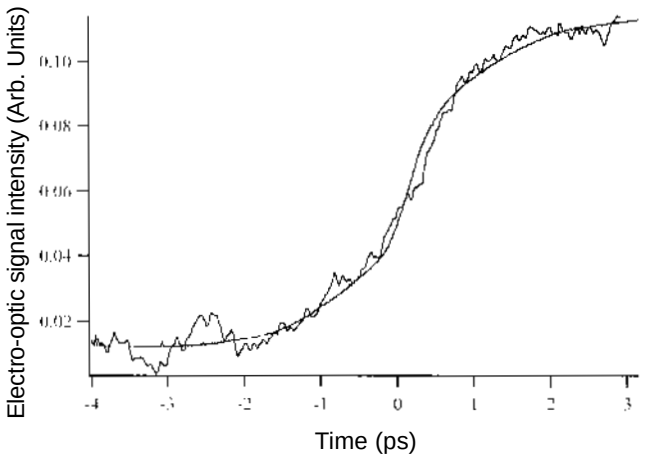

Figure 5. Reflective electro-optic sampling data for n-GaAs (100)/oxide interface (doping 7.8×10^{17} cm^{-3}). The photocarrier injection level was 4×10^{17} cm^{-3}. The electro-optic signal is shown in addition to a 200-fs fit for the rise time.

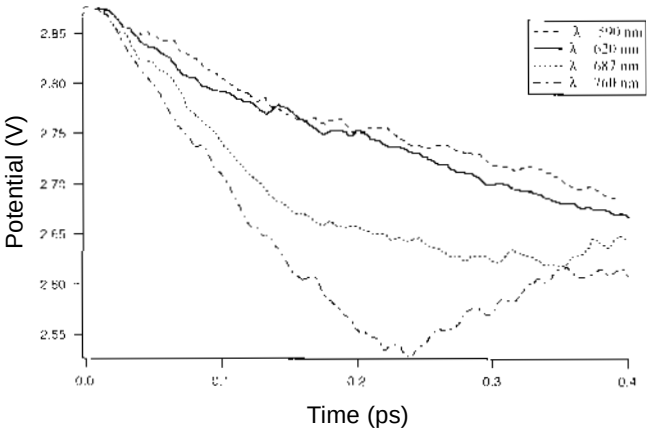

Figure 6. Monte Carlo simulation of optical excitation of GaAs: excitation energy dependence. The potential versus time at various excitation energies is shown. Note that the 590-nm injection pulse simulation corresponds to the experimental conditions in Fig. 5. Both the magnitude and dynamics are in relatively good agreement with experiment.

dynamical measurements at surfaces for this problem, which is free of transport limitations.

Charge Transfer. One of the most important fundamental issues related to interfacial charge transfer is the

degree of electronic coupling between the extended (highly delocalized) states of the solid state and the discrete electronic states of the molecular acceptor. The assumption generally made is that the mixing between states is weak and one can properly treat the problem using first-order perturbation methods, such as are implicit in the use of Marcus', Gerischer's, and other theoretical treatments.[26–30] For conventional electrochemical studies, the observable generally is treated as a steady-state current determined by the rate-determining process of the entire electrochemical cell. In this case, the use of first-order perturbation methods are justified. The spatial distribution of acceptors contributing to the current, electrode surface conditions (contaminants), or energetics will invariably lead to a rate-limiting step well approximated by weak electronic interactions between the acceptors and the electrode surface. However, these general trends do not mean that the electronic coupling is fundamentally limited to weak coupling conditions. It is clear from UHV surface studies that the electronic coupling between the surface and the molecular species can vary anywhere from chemisorption, where the electronic mixing leads to bond formation, to weakly physisorbed states.[31–34] Furthermore, Schmickler has shown by using a quantum mechanical treatment based on the Anderson-Newns model for adsorption and typical electronic couplings found in self-exchange reactions (homogeneous electron transfer) that electronic coupling should be found more generally in the strong, adiabatic coupling limit for heterogeneous electron transfer.[9] If this is indeed the case, electron-transfer dynamics could be extremely fast at surfaces rather than the slow electron limit assumed by first-order treatments.

Determining which general limit best describes the degree of electronic mixing at surfaces is extremely important in fully optimizing interfacial charge transfer. For example, if adiabatic coupling conditions can be designed into interfacial systems, it should be possible to attain 66% solar-to-electrical conversion efficiencies in solar cell designs.[35] This theoretical upper limit is based on electron transfer occurring faster than carrier thermalization such that energy is not lost to heat in the charge transfer/separation. This issue has been a controversial point and hinges on understanding a very fundamental aspect of the surface-reaction coordinate: the degree of wave-function overlap.

The most direct experimental probe of the relative degree of electronic coupling is to study the interfacial charge-transfer dynamics. The experimental challenge is to obtain a probe of the fastest steps in the reaction coordinate and not the rate-limiting process. To accomplish this goal, the reaction has to be prepared at the adiabatic crossing point so that nuclear-activation barriers do not dominate the observed dynamics. Another way to understand this conditional statement is that electronic coupling manifests itself only at the adiabatic crossing point (and modifies the nuclear-activation barrier under very strong coupling conditions). The adiabatic crossing point is the transition state region in the electron-transfer problem such that the challenge is to access information on the barrier-crossing dynamics in this region. However, this objective requires less than 10^{-2} monolayer sensitivity for surface studies and 100-fs time resolution. It is this combination of high sensitivity and time resolution that has prohibited significant progress in the past.

Surface Grating Studies of Carrier Reaction Dynamics. The above electro-optic sampling studies illustrate that optically preparing a surface population of reactive carriers within the prerequisite 100-fs time scale is possible. In principle, one could monitor the disappearance of these reactive states or the appearance of products using pump/probe spectroscopies. However, the sensitivity is not sufficient. A new method based on the transient-grating approach was developed to get around the sensitivity limitations of linear spectroscopies.[36,37] This method is an optical interferometric method. Two ultrashort, above-bandgap excitation pulses are made time coincident and crossed at an angle to generate an interference pattern on the surface. This pattern becomes encoded on the surface in the form of electron–hole pairs that modulate the index of refraction through free-carrier intraband transitions. A 3-D representation of the grating is shown in Fig. 7. The signal is derived from a third variably delayed probe beam diffracted off this grating image. The probe wavelength is chosen to be well off the resonance of the bandgap transition to selectively probe the carrier population. The diffracted signal is spatially isolated from all the other beams such that this experiment is as close as one can get to zero background in an all-optical experiment. This low background imparts the necessary sensitivity to conduct surface studies (signal-to-noise ratio is 1:1; 10^{-4} monolayer of reactive flux is detectable).

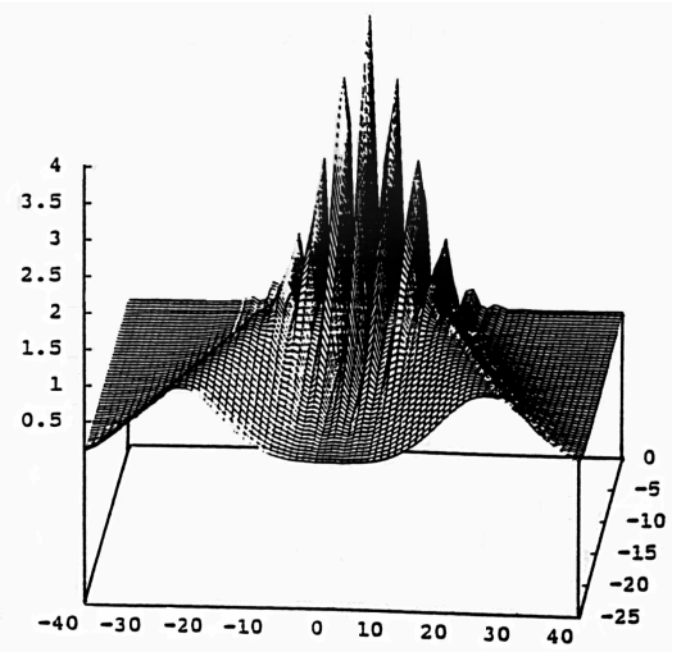

Figure 7. Three-dimensional representation of the optical intensity pattern produced at the sample surface by the interference of two excitation pulses. Electron–hole pairs are generated in this pattern leading to index of refraction changes and the formation of a diffraction grating. The carrier dynamics are monitored by diffracting a subbandgap probe off this grating.

The observable in the experiment is the diffracted probe intensity η which is defined by

$$\eta = \left\{ a\left(\frac{1}{m^*_e} + \frac{1}{m^*_h} \right) \int_0^\infty \Delta N(z,t)\, dz \right\}^2 ,$$

where a is a constant that depends on the probe wavelength and bandgap energy; $\Delta N(z,t)$ is the time-dependent grating peak–null spatial variation in electron and hole carrier number density parallel to the surface; z is the distance along the surface normal; and m^*_e and m^*_h are the effective electron and hole masses, respectively. This equation is given to illustrate that the diffraction efficiency

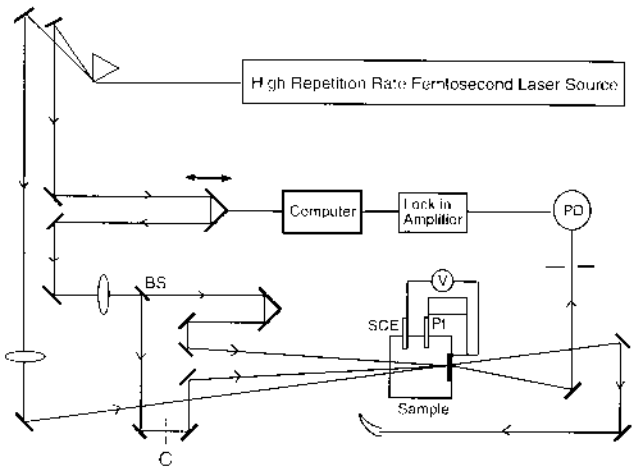

Figure 8. Experimental setup for surface-restricted transient grating: D = variable optical delay, BS = 50/50 beamsplitter, C = mechanical chopper, PD = photodiode, SCE = saturated calomel reference electrode, and Pt = platinum counterelectrode.

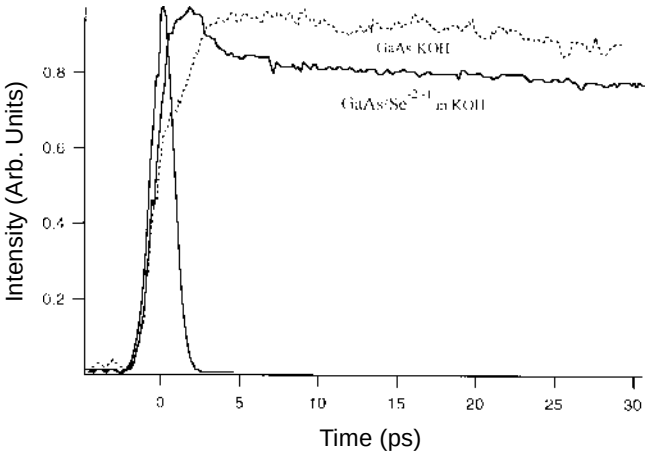

Figure 9. Grating studies of n-GaAs (100)/KOH aqueous liquid junction. Pulse autocorrelation is shown at $t = 0$. The solid decay represents the case where $Se^{-2/-1}$ redox couple is present in the solution. In comparison to the dashed decay representing absence of the redox couple, a fast 1- to 2-ps decay component exists that corresponds to hole transfer to the selenium acceptor. In fact, in the absence of selenium, there is a slower rising component attributed to the surface-state trapping of hole carriers. The decay component is approximately 20%, which represents the hole contribution to the signal.

η depends on the integrated (total) electron and hole carrier populations.

A key feature of the experiment is the explicit use of the surface space-charge field to give a surface population or surface grating component to the signal (as depicted in Fig. 3 for the surface-population dynamics). By changing the field polarity or type of doping and molecular acceptor, selectively monitoring and assigning the carrier charge-transfer dynamics to either electron or hole processes is possible. The other feature of the experiment is that by conducting a fringe-spacing dependence (by changing the angle between the grating excitation/writing beams), it is possible to verify that the signal originates from mobile charge carriers, i.e., carrier motion parallel to the surface contributes to the decay in the grating image. Large fringe spacings typically are used to minimize this contribution to the signal but it does serve as a useful diagnostic.

Surface-restricted grating spectroscopy was used to study interfacial hole transfer at the n-GaAs (100)/$Se^{-2/-1}$ aqueous liquid junction.[36] This system exhibits essentially unit quantum yield for charge transfer and is one of the few surfaces stabilized against oxidative photodegradation. Most important, with minimal surface preparation, this simple liquid contact exhibits ~15% solar energy conversion efficiencies which for single junctions is comparable to the best engineered solid state junctions. In addition, Se^{-2} is a well-known hole acceptor. The energetics are nearly isoenergetic with the valence band edge and Se^{-2} is strongly physisorbed to the surface with close to monolayer coverage. These conditions are ideal for determining the degree of electronic coupling achievable at semiconductor surfaces, and this system serves as an important test case.

The general experimental set up is shown in Fig. 8 for a three-beam configuration. Surface grating studies using a more elaborate four-pulse sequence demonstrated that interfacial hole transfer occurs with a $1/e$ time of 1 to 2 ps (Fig. 9).[36] This observation is the fastest resolved interfacial charge transfer (emission case) measured to date. The observed dynamics are faster than the diffusive reorientational dynamics of the highly charged aqueous double layer. Thus, the interfacial charge transfer is faster than one of the main components in nuclear relaxation along the reaction coordinate. In addition, the charge motion across the interface occurs in competition with scattering processes in the solid state that direct the electron along nonreactive electronic surfaces (k and r space), i.e., various scattering mechanisms displace the carrier both spatially and energetically away from the reaction saddle point. The fact that the dynamics are very close to even the fastest solvent relaxation modes illustrates that electronic coupling can occur in adiabatic regimes. This finding constitutes a new conceptual basis for engineering interfaces and is consistent with Schmickler's analysis of the interfacial electronic coupling. This finding also illustrates that conventional treatments of interfacial charge transfer using the assumption of weak coupling are not valid for photoinduced charge-transfer processes. Higher order theories are clearly needed. The most important single message from this work is that interfacial charge-transfer processes can be extremely fast (picosecond to femtosecond time scales) if the interface energetics are fully optimized.

Time Correlated Single Photon Counting Studies of Surface Quantum Wells. Time-correlated single-photon counting is a well-established technique to measure fluorescence decays.[38] It is one of the most sensitive photon detection techniques offering time resolution down to 10 ps. In addition, with proper use of a standard, the technique enables determination of absolute quantum yield as well. Single-photon counting is based on the concept that the probability distribution for emission of a single photon after an excitation event yields the intensity versus time distribution of all photons emitted due to that excitation. This probability distribution is obtained by sampling a single-photon emission following a large number of excitations.

The experimental apparatus is shown in Fig. 10. Time resolution is obtained by timing a fluorescence photon with respect to the excitation pulse. A picosecond laser pulse provides a trigger signal as well as optical excitation for the sample. The trigger pulse is detected with a photodiode and directed to a time-to-amplitude converter (TAC) as a "start" pulse to initiate charging of a capacitor. Meanwhile, the sample is excited and subsequently fluoresces. This fluorescence is collected such that at most one photon is detected for each excitation event. Detection is usually performed with a microchannel-plate-photomultiplier

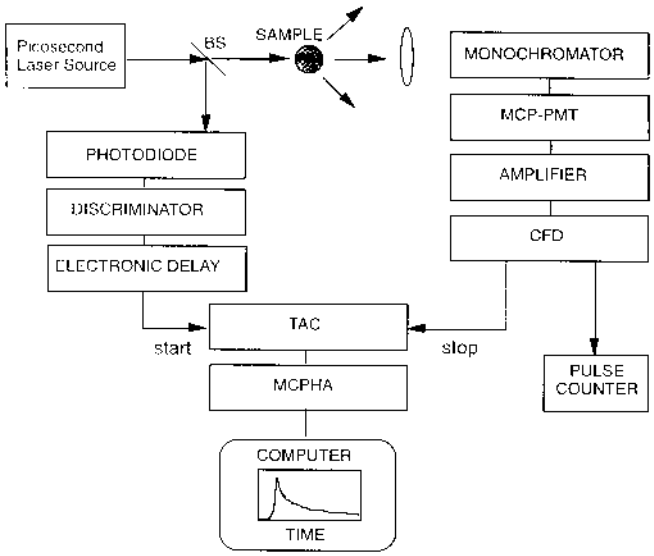

Figure 10. Experimental setup for time-correlated single-photon counting. BS = beamsplitter, MCP-PMT = microchannel plate photomultiplier tube, CFD = constant fraction discriminator, TAC = time-to-amplitude converter, and MCPHA = multichannel pulse height analyzer.

tube (MCP-PMT), and the signal is routed through various electronics to the TAC as a "stop" pulse to halt the charging ramp. The TAC then generates an electrical pulse proportional to the charge of the capacitor and, hence, the time difference between the start and stop pulses. Subsequently, a count is stored in the appropriate time channel in a data file. This process is repeated to build up a histogram of counts versus time. The instrument response is deconvolved from the data by collecting a time profile of the excitation pulse scattered off the sample. Ultimately, the instrument response is limited by the electron transit time spread between the photocathode and the MCP as well as the electron pulse spread during the multiplication process.[39] By using the PMT as a timing device, single-photon counting eliminates many of the distortions associated with photomultiplier detection and accompanying electronics. In addition, amplitude jitter is inconsequential as long as the pulse shape remains constant. These factors give single-photon counting the advantages of digital signal processing. Further, as this technique requires low emission intensity, it has become popular for probing weakly emitting samples.

This method does not have the time-resolution capabilities of the surface grating approach (~10 ps) but has comparable sensitivity. The main problem in radiative probes is that radiative recombination is blocked by surface fields such that surface dynamics are generally inaccessible. To get around this problem, surface quantum wells were used so as to ensure electron and hole wavefunctions overlap and radiative recombination selectively occurs at the surface. In this manner, the radiative lifetime of GaAs structures in contact with a molecular acceptor has been studied.[40,41] Electron transfer manifests itself by quenching the photoexcited population and, hence, altering the decay of the radiative recombination. The electron-transfer cross section for electron transfer from the semiconductor to a molecular acceptor can be obtained by observing the change in the radiative lifetime as a function of the acceptor concentration at the surface. The GaAs (100) surface quantum well samples are shown schematically in Fig. 11. Here confinement results from a heterojunction with $Al_{0.4}Ga_{0.6}As$ (100) on one side and the sample surface

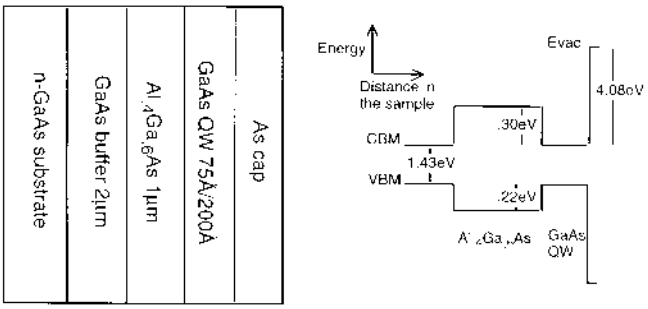

Figure 11. Schematic of GaAs (100) surface quantum well structures. The individual layers and corresponding thickness are shown on the left, while the associated energy is on the right. The CBM (conduction band minimum), VBM (valence band maximum), and E_{VAC} (vacuum level) for GaAs are shown.

on the other side. This structure was specially engineered to eliminate transport effects from the dynamics and was fabricated by molecular beam epitaxy (MBE)[42] to provide a high-quality surface important in minimizing surface defects. The surface consisted of either 75-Å or 200-Å GaAs (100) capped with a layer of amorphous As to prevent oxidation of the GaAs surface quantum well. This As cap was removed by heating the sample to 400°C for 15 min under high vacuum (10^{-7} torr) in a stainless steel cell prior to each experiment. This provided a clean surface with relatively few surface states for the ensuing experiments.

The above surface grating studies illustrated that charge transfer to strongly physisorbed acceptors is fast and essentially adiabatic. In electrochemistry, weakly physisorbed outer-sphere acceptors are usually employed for better mass transport and higher currents. Since this class of acceptors is weakly bound to the surface and potentially solvent separated from the surface, the electronic coupling is expected to be less than that for strongly physisorbed acceptors such as Se^{-2}. The aim of this study was to observe electron transfer in situ from GaAs to weakly physisorbed acceptors (outer-sphere acceptors) and thereby determine which regime of electronic coupling comes into play for this important class of acceptors. In these experiments, the GaAs quantum well was kept in contact with a well-known outer-sphere molecular acceptor: ferricenium tetrafluoroborate ($Fc^{+}BF4^{-}$) in acetonitrile. The GaAs (100) quantum well fluorescence decay was monitored while the quantum well interface was exposed to various concentrations of ferricenium (Fig. 12). Relative to the controls, the photoluminescence decay became about 30% faster in the presence of 10^{-2} M Fc^{+}, indicating that the electrons in the semiconductor were being depleted quicker. Hence, more concentrated solution increases the branching ratio of the electron transfer channel to the molecular acceptor. The coupling between the extended band states and discrete molecular states must be appreciable to affect the photoluminescence decay rate. An estimate of the electron capture cross section is in the range of 10^{-15} to 10^{-16} cm^{-2}, which indicates that photoinduced charge transfer can also approach adiabatic coupling for even outer-sphere acceptors.

Carrier Thermalization. Photogenerated hot, nonequilibrium carriers thermalize rapidly via various mechanisms where impurities, defects, phonons, and charge carriers themselves are scattering sources. These dynamics are critical to interfacial charge transfer as they offer a competing reaction pathway to charge transfer and also serve to localize the charge in the solid state half space. Further, thermalization represents hot-carrier energy loss. Boudreaux, Williams, and Nozik proposed a hot electron-transfer model for semiconductor/electrolyte junctions

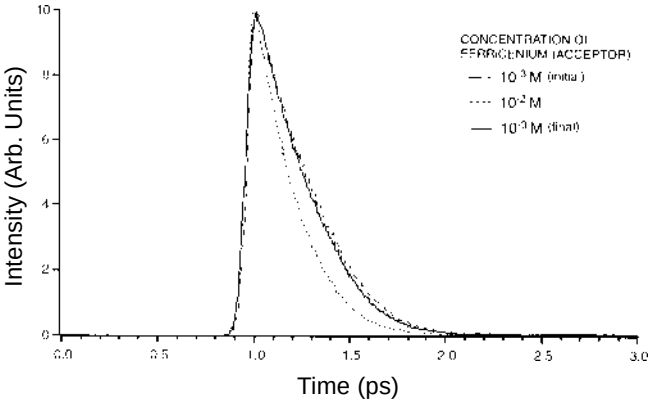

Figure 12. Single-photon counting studies of GaAs (100) 75 Å/$Fc^{+1/0}$ interface. Concentration dependence of the photoluminescence decay is shown. The lifetime reduction at higher concentration (10^{-2} M, dotted line) is attributed to an increase in the branching ratio of the electron transfer channel. On reinserting the dilute solution (10^{-3} M, solid line), the decay returns close to the original dashed-line decay showing that the ferricenium acceptors weakly physisorb to the surface owing to their outer sphere nature.

where minimizing thermalization energy loss enhances the maximum theoretical conversion efficiency to 66%, double that of an all solid state junction.[35] This model has been much debated because it requires electron transfer to occur faster or at least in competition with electron relaxation. Hence, measurement of the dynamics and energetics of carrier relaxation are crucial to determining the feasibility of this model.

Recent experiments have optically probed semiconductors to examine relaxation dynamics. Transient transmission,[43–47] transient reflection,[48] time-resolved luminescence,[49–52] and degenerate four-wave mixing[53–60] spectroscopies have been applied to this problem and have yielded valuable information. However, they cannot directly access hot-carrier dynamics relevant to surface photochemistry. In this respect, electrons with excess energies of ~1 eV (comparable to field-accelerated electrons), within the first 100 Å need to be probed. The above techniques measure changes in the optical properties of the sample and relate these to electron dynamics that are not well defined for high energies. The photoluminescence methods also lack the time resolution and/or sensitivity to access these electrons. In addition, most of these techniques are limited to probing bulk processes whereas at the surface, the dynamics can be significantly altered due to broken symmetry (which affects the local density of states and perturbs the phonon distribution) and the relatively high defect density arising from surface states. Time-resolved electron photoemission overcomes these shortcomings and is currently the technique of choice to time and energy resolve electron dynamics at surfaces.

Time-resolved two-photon photoemission is basically a pump–probe technique (Fig. 13). The first photon $h\nu_1$ (pump) excites an electron from the valence band into the conduction band creating a density of photoexcited electrons. A variable time later, the second photon $h\nu_2$ (probe) further excites these electrons above the vacuum level from where the charge carriers are detected. By knowing the photon energies and the electron affinity of the semiconductor, the photoemitted electrons can be directly mapped on to the excited electron distribution Hence, the population of an intermediate state is monitored and by varying the time between the pump and probe pulses, the lifetime of that state can be extracted. Using femtosecond pump and probe pulses provides femtosecond time resolution.

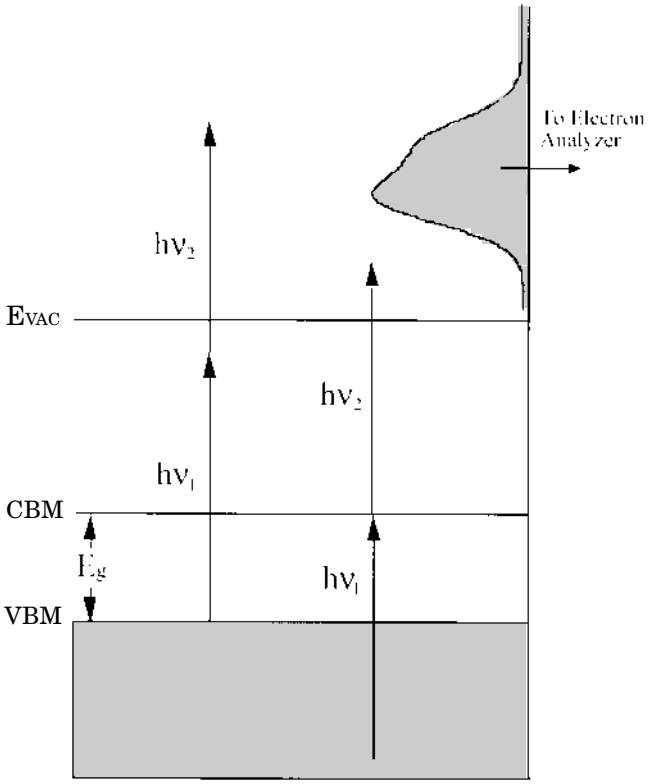

Figure 13. Simplest representation of two-photon photoemission spectroscopy. CBM, VBM, and E_{VAC} denote the conduction band edge, valence band edge, and vacuum level, respectively, with bandgap, Eg. The electron distribution that is excited above the vacuum level is detected with an electron analyzer. This technique enables monitoring the population of a given energy level in the conduction band.

Surface sensitivity is automatically achieved by detecting photoemitted electrons; only the electrons within the escape depth of the sample can be measured. This escape depth is material dependent and is of the order of 100 Å for GaAs. Hence, time-resolved two-photon photoemission allows simultaneous measurement of the dynamics and energetics of electron relaxation with high surface sensitivity. This has been applied to the measurement of electron relaxation at semiconductor as well as metal surfaces.[61–68] The obvious drawback of time-resolved photoemission is the requirement of ultrahigh vacuum conditions to detect electrons.

We have utilized time-resolved two-photon photoemission, with 10 to 15-fs time resolution and 0.1 to 0.2-eV energy resolution, to study both bulk GaAs (100) and surface quantum well systems (described earlier in this report, Fig. 11). Decapping the quantum wells under ultrahigh vacuum conditions provided a pristine surface with minimal surface states. The experimental schematics of the setup are shown in Fig. 14. The setup consists primarily of a femtosecond laser system and an ultrahigh vacuum chamber equipped with a hemispherical energy analyzer. Experimental details are provided elsewhere.[68] At high excitation energies (2.0-eV case) the dynamics are considerably fast, around 60 fs, and are well described by a single exponential. However, as the energy decreases the decay becomes more Gaussian indicating the presence of an electron source term. This was the first direct observation of the cascading mechanism. This mechanism is most prevalent at intermediate and low excess energies whereby electrons relax from higher energy states to populate the lower lying intermediate and low-energy states.

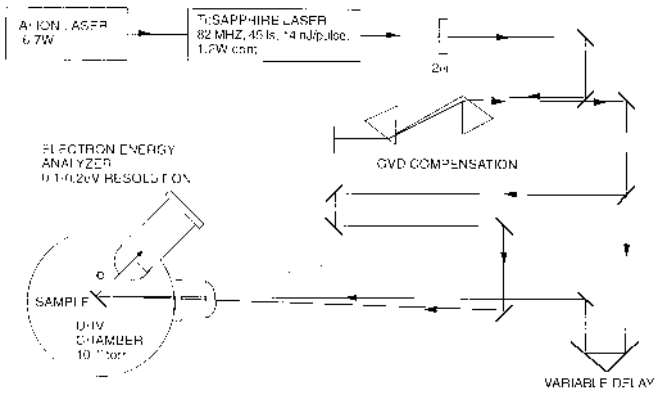

Figure 14. Experimental layout for time-resolved two-photon photoemission. 2ω = frequency doubling crystal, BS = beamsplitter, and GVD = group velocity dispersion (which is compensated by using a prism pair). The variable delay controls the time between the pump and probe pulses.

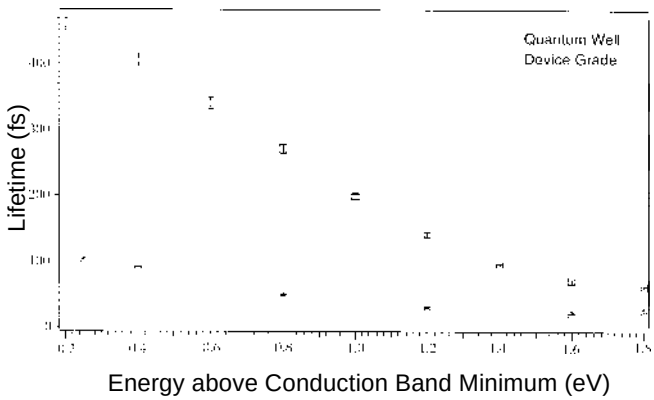

Figure 15. Excited-state dynamics as a function of energy. The device-grade bulk GaAs exhibits considerably fast relaxation even at low-excitation energies (100 fs at 0.4eV) and is similar to that of metals at high energies (20 fs at 2.0 eV). For the 200-Å QW, the lower defect density in the MBE-grown sample slows down the dynamics at lower energies (450 fs at 0.3 eV) and with increasing energy the electron lifetime decreases approaching that of the bulk material.

These lifetimes are depicted as a function of energy of the electron distribution in Fig. 15. These experiments were also performed on melt-grown device-grade GaAs (100) samples (Fig. 15). The dynamics were several times (approximately 5) faster than for the MBE-grown quantum wells ranging from 100 to 10 fs.

The main result of these experiments was that electron relaxation at GaAs (100) surfaces is a femtosecond process that shows significant material-quality dependence. With respect to the branching ratio or potential for using hot electrons, this work has now fully characterized electron relaxation at surfaces. It is clear from considering the interfacial dynamics discussed above that for low-defect surfaces, the hot electron-transfer channel can become competitive with electron relaxation—thereby enabling a future generation of highly efficient solar cells harvesting hot as well as thermalized electrons.

Electron Injection

The complementary process to electron emission is electron injection from a molecular species to a semiconductor. Dye sensitization has proven to be a molecular system that is efficiently probed optically. In recent years, much

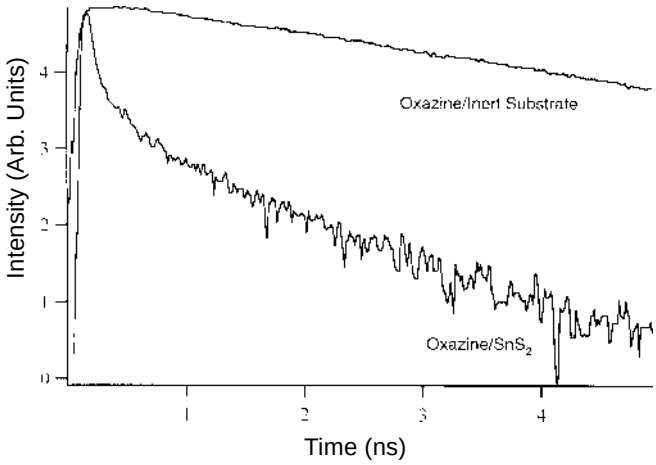

Figure 16. Time-resolved fluorescence from oxazine obtained with time-correlated single-photon counting. The slower decay corresponds to the dye on an inert cellophane substrate while the lower biexponential decay is from oxazine on SnS_2. Integration yields a fluorescence quenching ratio of $(9 \pm 5) \times 10^4$.

work has been done on electron injection at dye-sensitized semiconductor surfaces using a variety of semiconductors.[69–80] However, in most of these studies, electron injection rates ranging from 50 to 2000 ps have been measured. These slow rates are probably a consequence of weak electronic coupling between the dye and the substrate due to poor surface quality and high surface state density.

In this regard, SnS_2 has excellent surface properties.[81] SnS_2 is a flat, atomically smooth, layered semiconductor with few surface states. By virtue of its 2-D nature, bonds are terminated in each layer leading to a chemically inert surface. The high surface quality enables strong electronic coupling between the sensitizing agent and the semiconductor, without the interference of surface-state processes with direct electron injection. This is reflected in high quantum yields, close to 80% for electron transfer and collected current at SnS_2 surfaces.[81] In addition, the large 2.2-eV indirect bandgap facilitates exclusive excitation of the dye-sensitizing agent such that the molecular excited state is isoenergetic with the electronic states of the conduction band.

Oxazine-1-sensitized SnS_2 was chosen as a model photosensitized system to probe electron injection. This dye has negligible dimer formation even at fairly high concentrations which permits strong coupling at the interface without complications arising from dimer formation.[82] The oxazine ground state is midgap in energy and its first singlet state is approximately 0.35-eV above the conduction band edge leading to barrierless electron injection. It is desirable to measure both forward as well as backward electron-transfer rates to fully understand the high quantum yields at SnS_2 surfaces.

Fluorescence decays and quenching rate were measured with the time-correlated single-photon counting method described above.[80] Oxazine fluorescence was monitored on an inert reference substrate, cellophane tape, as well as on SnS_2 (Fig. 16). The former yielded a single exponential decay with a 2.6 ± 0.1 ns lifetime. The more complex decay curve of oxazine on SnS_2 was fit to a biexponential decay comprised of a fast instrument-limited 40-ps time constant and a longer 900 ± 100 ps decay. The longer decay exhibited concentration dependence and virtually disappeared at low coverage. This component was attributed to fluorescence from dye molecules that were weakly adsorbed or weakly electronically coupled to the surface. The fast instrument-limited decay was ascribed to the signal from

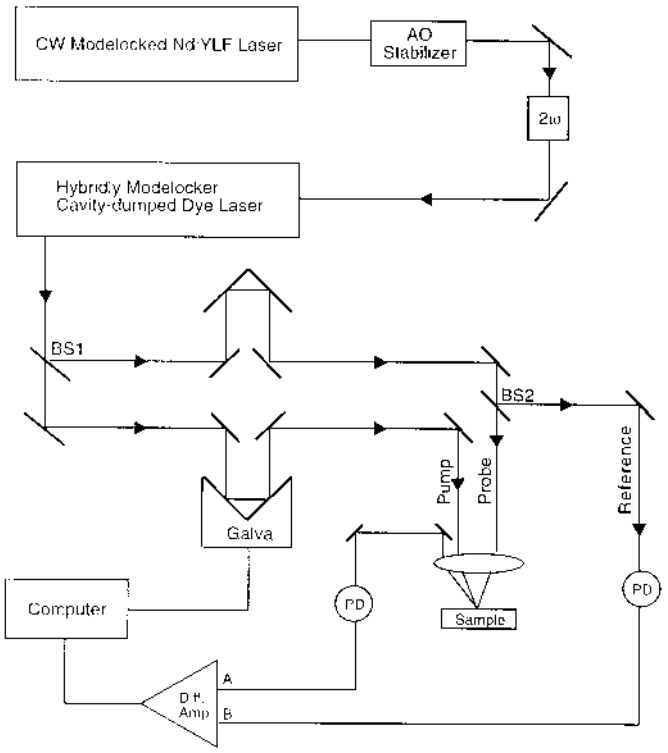

Figure 17. One-color pump-probe transient absorption experiment in reflection: experimental layout. 2ω = frequency doubling crystal, BS1 and BS2 = beamsplitters, 70% transmissive, Galva = galvanometer delay, PD = photodiode, and DA = differential amplifier.

molecules strongly coupled to the surface indicating that the electron injection rate is significantly faster than 40 ps. This decay component was unresolved but an estimate of the excited state lifetime was made by determining the fluorescence quantum yield, using the radiative rate as an internal clock. Studies of the integrated fluorescence intensity yielded a quenching factor of $(9 \pm 5) \times 10^4$. Assuming electron injection was the only additional nonradiative channel, this value implied a time constant of 40 ± 20 fs for electron transfer from the excited singlet state of oxazine into the conduction band of SnS_2.

To follow the carrier dynamics in real time and monitor the ground state recovery of oxazine (back electron transfer), a one-color pump–probe transient absorption measurement in reflection was performed on oxazine-sensitized SnS_2.[80] The back electron transfer is essential to determining the overall photocurrent yield. The experimental setup is shown in Fig. 17. The pump photon excites the dye molecules to the first excited singlet state partially photobleaching the absorption while the probe photons sample the same absorption. The absorption reflects the ground-state population of the sensitizing agent and, hence, allows measurement of the ground-state recovery when oxidized dye molecules and electrons from the semiconductor recombine. To directly monitor the transient absorption of a dye on a surface in this manner represents a challenge to attain the requisite sensitivity. The key technological advance that enabled these measurements was the use of a rapidly scanning galvanometer for high-speed data acquisition. This approach eliminated the dominant low-frequency laser noise from the experiment, and detection limits of less than 2×10^{-7} changes in probe transmission were possible.

Representative results are shown in Fig. 18. The signal appeared only when SnS_2 was sensitized. Hence, the signal was assigned to the bleaching of the ground-state absorption of oxazine by the pump pulse while the decay corresponded to the ground-state recovery. The dominant feature was a fast, approximately 10 ps, decay that appeared to be the ground-state recovery time. As these dynamics were significantly slower than the fluorescence quenching, the possibility of energy transfer to surface-state traps was eliminated. This finding further supports the assignment of the short (~40 fs) excited state lifetime to electron transfer.

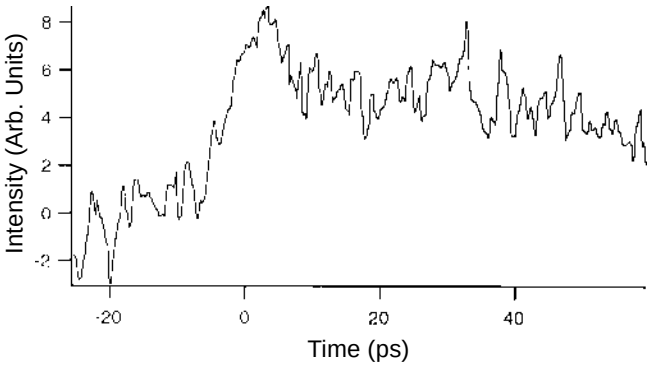

Figure 18. Ground-state recovery of oxazine on SnS_2 probed with one-color pump-probe transient absorption spectroscopy in reflection. The decay has a fast 10-ps component corresponding to back electron transfer from the semiconductor to the dye. There is also a longer position-sensitive component with time constant of several hundred picoseconds and relatively small magnitude. This is ascribed to the ground-state recovery of less strongly coupled dye molecules. The changes in probe transmission are on the order of 10^{-6}. This small signal detection is made possible with the galvanometer that permits the collection at repetition rates between 1 to 100 Hz and eliminates the dominant low-frequency laser noise below 1 to 10 Hz.

The most important feature of the above experiment is that both the decay of the reactant state (via fluorescence quenching) and the product state were observed. In the latter case, the product is the parent cation that creates a bleach in the ground-state absorption. If the short excited state lifetime inferred from these studies was due to energy transfer rather than electron transfer, the ground-state recovery would have been the same as the excited state decay (i.e., < 100 fs). The fact that the ground-state bleach is observed in the presence of a short-lived excited state, with a high quantum yield for photoinjection, strongly supports assigning the dynamics to interfacial charge transfer. These studies were the first to attain direct observation of submonolayer excited-state dynamics at a single crystal surface and were only possible with the advent of data acquisition methods to reduce the laser noise contributions to the signal. Similarly, fast dynamics have been observed for dyes on colloidal TiO_2 where the excited-state and cation parent transient absorption spectrum have also been measured.[4] The TiO_2 system has the advantage of a large surface area that reduces the sensitivity requirement by several orders of magnitude. The problem with this system is that it is not a single crystal surface but highly amorphous. The surface is really not defined and a wide range of dynamics have been reported. Colloidal TiO_2, however, harbors tremendous potential as a new solar cell material and a great deal of work has been devoted to understanding charge-transfer processes at this surface.

Note that the electron-transfer dynamics as inferred from the SnS_2/oxazine model system are extremely fast (~40 fs); faster than conventionally thought possible. Normally, electron transfer can not proceed faster than the

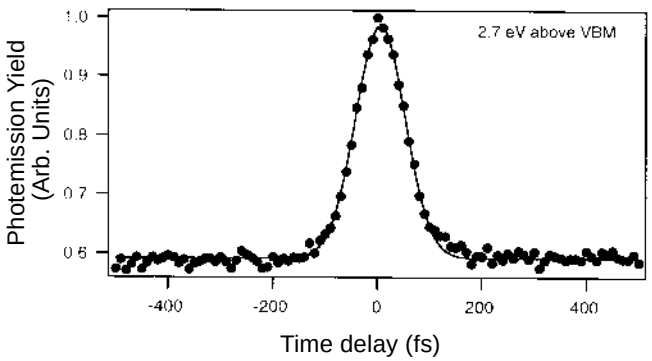

Figure 19. Pump-probe scan of SnS_2 using time-resolved two-photon photoemission at room temperature for orthogonal polarization of the pump and probe beams. This scan represents the electron population 2.7 eV above the valence band maximum. The data were fit to yield a relaxation lifetime of 25 fs.

nuclear relaxation along the reaction coordinate, i.e., faster than the nuclear motion needed to decouple the two electronic states undergoing electron exchange. This condition is only reached if and only if the electronic coupling is such that the electronic coordinate equilibrates faster than the nuclear motions (adiabatic limit). Dynamics in the range of 40 fs are generally considered to be faster than the key nuclear motions that dominate the reaction coordinate. However, it was shown to 4th order that for a dye in contact with a surface, the electronic continuum serves the same role as the nuclear relaxation in localizing the electron in the product channel (in this case, the conduction band).[80] The electron-transfer process can be purely electronic, and for dye molecules with excited state levels above the CBM, the electron-transfer dynamics give a direct probe of the electronic coupling. (For levels below the conduction band, a nuclear-activation barrier exists such that the dynamics become determined by the activation process and not the electronic coupling.) Extremely fast electron-transfer dynamics from other systems have been observed that further support this concept.[78]

The above ultrafast dynamics also suggest extremely fast electronic dephasing in the solid state occurs that is faster than typical nuclear relaxation. For SnS_2, this has indeed been the case, electron dephasing at room temperature in semiconductors is usually determined by electron–electron scattering and is usually less than 100 fs (scattering time) for typical conditions. In the case of SnS_2, not only does fast electron dephasing occur but also extremely fast electron thermalization (inelastic scattering process), fast enough to accommodate fast electron-transfer dynamics as suggested above. Representative results are shown in Fig. 19 for femtosecond photoemission studies of electron relaxation in this material. The electron thermalization dynamics occur within 20 to 60 fs, which is highly unusual. These relaxation dynamics are nearly the same as metals and most likely reflect the 2-D nature of the material (new channels occur through coupling to 2-D plasmons between layers.)[83]

This is an interesting set of observations which as in the case of *n*-GaAs (100) has now given us a complete description of the operating dynamics at SnS_2 interfaces. Currently, the exact energetics of the dye-excited state relative to the CBM need to be determined since different dynamics are reported for different dyes.[75,80] This information will help rationalize the differences. Regardless, the new concepts involving a purely electronic coordinate and the associated time scales for the operating dynamics at dye-sensitized semiconductor surfaces give a new fundamental basis for examining and optimizing imaging processes.

Summary and Future Outlook

Time-domain spectroscopies were utilized to probe surface reaction dynamics and characterize interfacial electron transfer, the fundamental process triggering virtually all light-driven imaging technologies. The study of the primary processes controlling the efficiency of interfacial charge-transfer dynamics required ultrafast optical experiments with high surface sensitivity. Two complementary initial conditions for electron transfer at surfaces were experimentally investigated. The GaAs/electrolyte model system was used to study electron emission (where the electron is optically prepared in the solid state and transferred to molecular acceptors on the liquid half space of the interface). On the other hand, dye-sensitized SnS_2 surfaces were studied to follow electron injection (where the electron is initially localized on the molecular donor and injected into the semiconductor). Essentially all the photophysical processses controlling the electron-transfer coordinate for these two model interfaces were characterized near or at the reaction saddle point. These dynamics are summarized in Fig. 20.

As appreciated from Fig. 20, we now have a fairly comprehensive real-time view of interfacial electron transfer. In this endeavor, several new spectroscopies were developed that have gained access to certain aspects of the electron transfer reaction coordinate inaccessible with conventional methods. Now possible is the observation of the fastest processes controlling efficiency and product distribution of interfacial electron transfer rather than just the rate-limiting processes. In essence, the time-resolution limits are now in the 10- to 100-fs range such that even the transition-state processes of barrier crossing can be followed, i.e., the fundamental upper limit to the electron-transfer dynamics can be studied. In many cases, the observed dynamics are in a range where we need to recalibrate our thinking about the operational time scales of the primary processes controlling interfacial electron transfer. This comment is made with respect to both nuclear and electronic factors. In the case of nuclear factors, we now know that the solvent coordinate contains nondiffusive components in the 100-fs range that contribute substantially to nuclear relaxation.[4,84,85] This motion is nearly an order of magnitude faster than expected based on continuum treatments of dielectric relaxation to model the solvent motion along the reaction coordinate. With respect to electronic factors, the most important information gained from the studies of the electron emission at GaAs (100)/electrolyte interfaces is that the charge-transfer process can occur on time scales consistent with adiabatic coupling conditions between the band states and the discrete molecular acceptors at the interface. This condition holds true for both strongly and weakly physisorbed outer-sphere acceptors. These observations indicate that the electron probability distribution of the solid state wave function penetrates sufficiently past the first solvent layer to yield strong mixing conditions with molecular acceptors (providing the energetics are optimal) within the double layer. Consistent with this view, extremely fast electron-injection dynamics were observed for weakly physisorbed dyes at SnS_2 interfaces (oxazine reversibly adsorbs to SnS_2 surfaces). The dynamics in this case were in a range faster than the relevant nuclear relaxation processes (i.e., adiabatic) and illustrated that the electron could be transferred or localized in the solid state through purely electronic processes.

The single most important finding from these collective works is that interfacial electron-transfer processes can occur in the picosecond to subpicosecond time domain in a range consistent with adiabatic coupling conditions, which is a major departure from conventional treatments of this

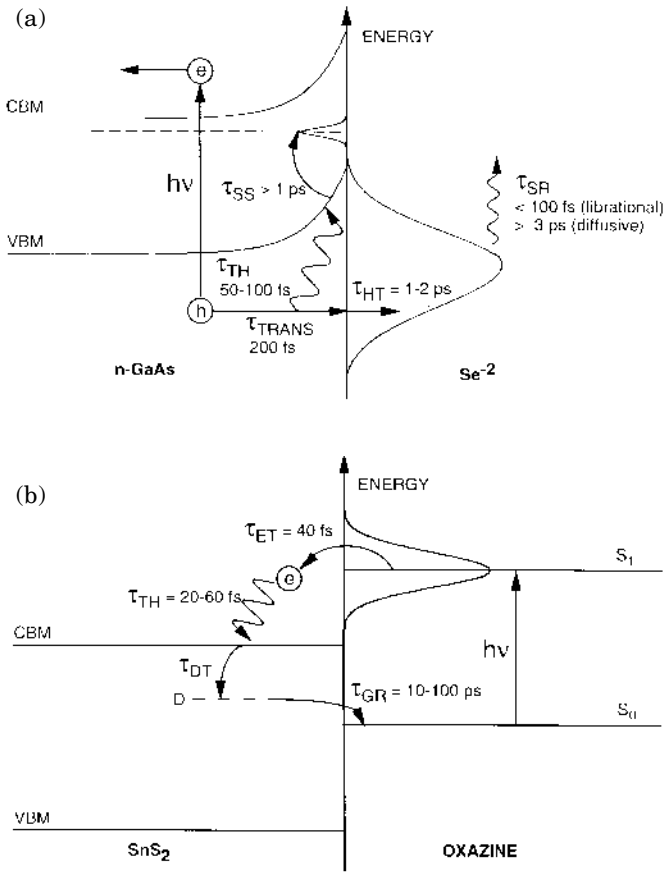

Figure 20. A. Photophysical processes for electron emission (*n*-GaAs (100)/$Se^{-2/-1}$ aqueous liquid junction). Electron transport has been characterized by electro-optic sampling indicating that carriers are accelerated from within the space-charge region to the surface in 200 fs (τ_{TRANS}) and arrive hot at the surface. The energetics and dynamics of electron relaxation has been determined with femtosecond two-photon spectroscopy (τ_{TH}). For electrons with 1 eV of excess energy, the relaxation is exceedingly fast (< 100 fs). Surface-restricted transient grating spectroscopy probed the subsequent interfacial charge transfer (τ_{HT}) and measured these dynamics to occur in 1 to 2 ps, approaching time scales associated with adiabatic coupling (which defines the upper limit to electron transfer dynamics for electron emission). In competition with this direct charge transfer step is that of surface-state trapping (τ_{ss}) which is dynamically limited to time scales longer than 1 ps by carrier cooling. The nuclear relaxation processes (τ_{SR}), mainly determined by the solvent coordinate, involve nondiffusive motions (<100 fs) and diffusive reorientational water motions (>3 ps, high ion concentration of double layer) placing the observed dynamics in the adiabatic limit. Similar electron transfer cross-sections have been obtained for GaAs in contact outersphere reagents, indicating that adiabatic conditions can be reached for both weakly and strongly physisorbed acceptors. B. Photophysics for electron injection (SnS_2/oxazine). Single-photon counting and integrated fluorescence studies of oxazine-sensitized SnS_2 have indicated extremely fast electron transfer times (τ_{ET}) of 40 fs. Here the quasi continuum of the solid state serves to localize the electron in the product channel. Two photon photoemission studies on SnS_2 have shown extremely fast electronic dephasing and relaxation (down to 20 fs). The short lifetime observed for oxazine is consistent with this concept and provides a direct measurement of the electronic coupling. This finding illustrates that for even weakly physisorbed acceptors the electronic coupling can be in the adiabatic limit, consistent with similar observations for electron emission. The subsequent back electron transfer (τ_{GR}), resolved with surface-sensitive transient absorption spectroscopy, had multicomponents from 10 to 100 ps. This relatively slow back transfer partly explains the large quantum yield for electron separation at this surface.

process. Note, however, determining whether the degree of electronic coupling is sufficient to modify the nuclear-activation barrier is not possible. The above picture can still be supported within a weakly adiabatic description of the electron-transfer coordinate.[4,9] Nevertheless, these observations illustrate that photoinduced electron-transfer processes are not determined by the same factors that control electrochemical processes. The involvement of a photon in the process promotes the system much farther from equilibrium than thermal fluctuations near the Fermi level of a metal electrode. In the photoinduced case, molecules in direct contact with the surface, and strongly mixed with the band states, determine the electron-transfer observables. One cannot simply apply the weak-coupling assumption used in conventional treatments of interfacial charge transfer in electrochemical processes to the photoinduced electron-transfer processes involved in imaging. More rigorous theoretical treatments of the interfacial reaction coordinate are required to understand these implications fully.

From a practical standpoint, this new insight into interfacial charge transfer may lead to new approaches for maximizing the charge-separation efficiency based on semiconductor/molecular (donor/acceptor) architectures. For example, the electron-emission dynamics taken together with the studies of carrier thermalization illustrate that interfacial charge transfer can occur on time scales competitive with carrier thermalization. This finding supports the general ideas behind the hot-carrier model for solar cell designs that avoid heat loss in the overall conversion efficiency.[35] With respect to electron injection, the electron dynamics are fast enough to be promoted purely by electronic factors where solid state scattering and thermalization assist the charge separation. Prior to the development of femtosecond laser spectroscopies capable of following these processes, solid state dynamics were always treated as being too fast and decoupled from the problem. With these latest advances, we now see that hybrid semiconductor/molecular interfaces can be designed to have properties and dynamics approaching all solid state interfaces. New approaches to optimally engineering interfaces to exploit and control the electronic and nuclear factors controlling the overall efficiency are foreseeable.

A whole battery of new techniques have been developed to address different aspects of the interfacial electron-transfer reaction coordinate. These methods in conjuction with other time-domain approaches should serve as useful tools in fully understanding interfacial systems and refining our control over their properties. As can be seen from Fig. 20, virtually all the relevant dynamics and photophysical processes controlling imaging process can now be probed with 100-fs time resolution and high sensitivity. In addition, femtosecond laser technology has matured to the point that reliable commercial systems are now available such that the laser technology should no longer represent an impediment to extending these studies to other systems. A clear future direction for this research is to extend this work to obtain a real-time view of the photophysical and photochemical processes involved in the imaging process—a real-time view of the photographic process in silver halides. This is one of those "holy grails" of science. With the large number of model dye systems and interfacial energetics available from photographic research, work in this area may ultimately lead to a fully quantum description of interfacial electron transfer at surfaces. In this regard, the technical motivation for understanding the photographic process in detail may lead to our most fundamental understanding of heterogeneous electron transfer, in general. ▲

Acknowledgments. This work was supported by DOE, the NSF Science and Technology Center for Photoinduced Charge Transfer, and the Natural Sciences and Engineering Council of Canada (RJDM). SJD acknowledges support from the Link Energy Research Foundation. The work discussed in this article is the result of a number of fruitful collaborations over the years. The authors would particularly like to acknowledge discussions with A. A. Muenter, Y. L. Gao, D. Mantell, C. Schmuttenmaer, C. C. Miller, S. Xu, J. Lanzafame, L. Gomez-Jahn, D. Wang, S. Mukamel, B. Parkinson, A. Nozik, and F. Willig that have contributed greatly to the concepts put forward in this article.

References

1. T. H. James, Ed., *The Theory of the Photographic Process*, 4th ed., MacMillian, New York, 1977.
2. E. M. Williams, *The Physics and Technology of Xerographic Processes*, John Wiley & Sons, New York, 1984.
3. J. H. Dessauer, Ed., *Xerography and Related Processes*, Focal Press, New York, 1965.
4. R. J. D. Miller, G. McLendon, A. Nozik, F. Willig, and W. Schmickler, *Surface Electron Transfer Processes*, VCH Publishers, New York, 1995.
5. S. R. Morrison, *Electrochemistry at Semiconductor Surfaces and Oxidized Metal Electrodes*, Plenum Press, New York, 1980.
6. H. O. Finklea, Ed., *Semiconductor Electrodes*, Elsevier, Amsterdam (1988).
7. C. A. Koval and J. N. Howard, *Chem. Rev.* **92:** 411 (1992).
8. N. S. Lewis, *Ann. Rev. Phys. Chem.* **23:** 176 (1990).
9. W. Schmickler, *J. Electroanal. Chem.* **204:** 31 (1986).
10. J. Lanzafame and R. J. D. Miller, *Ultrafast Dynamics of Chemical Systems*, J. R. Simon, Ed., Kluwer Academic Publishers, 1994.
11. J. M. Lanzafame, S. Palese, D. Wang, R. J. D. Miller, and A. A. Muenter, *J. Phys. Chem.* **98:** 11,020 (1994).
12. W. Kaiser, Ed., *Ultrashort Laser Pulses Generation and Application*, 2nd ed., Springer-Verlag, Berlin, 1993.
13. D. K. Evans, Ed., *Laser Applications in Physical Chemistry*, Marcel Dekker Inc., New York, 1989.
14. J. S. Blakemore, *J. Appl. Phys.* **53:** R123 (1982).
15. B. A. Parkinson, *Langmuir* **4:** 967 (1988).
16. B. A. Parkinson and M. Spitler, *Electrochim. Acta* **37:** 943 (1992).
17. S. M. Sze, *Semiconductor Devices: Physics and Technology*, John Wiley & Sons, New York, 1981..
18. J. A. Valdmanis and G. Mourou, *IEEE J. Quant. Electron.* **QE22:** 69 (1986).
19. B. H. Kolner and D. M. Bloom, *IEEE J. Quant. Electron.* **QE22:** 79 (1986).
20. L. Min and R. J. D. Miller, *Chem. Phys. Lett.* **163:** 55 (1989).
21. L. Min and R. J. D. Miller, *Appl. Phys. Lett.* **56:** 524 (1990).
22. (a) G. C. Cho, W. Kutt, and H. Kurz, *Phys. Rev. Lett.* **65:** 764 (1990); (b) L. Xu, Y. Chang, and H. W. K. Tom, *Quantum Electronics and Laser Science '95*, Summaries of Papers Presented, **16**, 1995.
23. X. Zhou and T. Y. Hsiang, and R. J. D. Miller, *J. Appl. Phys.* **66:** 3066 (1989).
24. X. Zhou and T. Y. Hsiang, *J. Appl. Phys.* **67:** 7399 (1990).
25. X. Zhou, Ph.D. Thesis, University of Rochester, 1990.
26. (a) R. A Marcus, *J. Chem. Phys.* **24:** 966 (1965); (b) R. A. Marcus, *Ann. Rev. Phys. Chem.* **15:** 155 (1964).
27. H. Gerisher, *Z. Phys. Chemie NF* **26:** 223 (1960).
28. H. Gerisher, *Z. Phys. Chemie NF* **27:** 40 (1961).
29. V. Levich and R. R. Doganodze, *Dokl. Akad. Nauk. SSSR*, **124:** 123 (1959).
30. A. N. Kuznetsov, in *Modern Aspects of Electrochemistry*, vol. **22**, B. E. Conway, R. E. White, and J. Bockris, Eds., Plenum Press, New York, 1990.
31. G. Schonhense, A. Eyers, and U. Heinzmann, *Phys. Rev. Lett.* **56:** 512 (1986).
32. P. Avouris, and R. E. Walkup, *Ann. Rev. Phys. Chem.* **40:** 173 (1989).
33. C. Schmuttenmaer, M. Aeschlimann, J. Cao, H. Elsayed-Ali, Y. Gao, D. A. Mantell, and R. J. D. Miller, in *SPIE Proc.* **2125**: 98 (1994).
34. J. A. Prybyla, H. W. K. Tom, and G. D. Aumiller, *Phys. Rev. Lett.* **68:** 503 (1992).
35. D. S. Boudreaux, F. Williams, and A. J. Nozik, *J. Appl. Phys.* **51:** 2159 (1980).
36. D. Wang, J. Buontempo, Z. W. Li, and R. J. D. Miller, *Chem. Phys. Lett.* **232:** 7 (1995).
37. L. A. Gomez-Jahn and R. J. D. Miller, *J. Chem. Phys.* **96**, 3982 (1992).
38. D. V. O'Connor, D. Phillips, *Time-Correlated Single Photon Counting*, Academic Press, London, 1984.
39. I. Yamazaki, N. Tamai, H. Kume, H. Tsuchiya, and K. Oba, *Rev. Sci. Instrum.* **56:** 1187 (1985).
40. S. Diol, C. Miller, J. Cao, Y. Gao, and R. J. D. Miller, *Conference on Electro-Optics/Quantum Electronics and Laser Science*, 1995, postdeadline paper QPD21.
41. S. J. Diol, C. C. Miller, Y. Gao, and R. J. D. Miller, *Ultrafast Phenomena X*, p. 402, (Springer-Verlag, Berlin, 1996).
42. Manufactured at the University of Rochester Molecular Beam Epitaxy Laboratory.
43. P. C. Becker, H. L. Fragnito, C. H. Brito Cruz, J. Shah, R. L. Fork, J. E. Cunningham, J. E. Henry, and C. V. Shank, *Appl. Phys. Lett.* **53:** 2089 (1988).
44. U. Hohenester, P. Supancic, P. Kocevar, X. Q. Zhou, W. Kütt, and H. Kurz, *Phys. Rev. B* **47:** 13233 (1993).
45. A. J. Taylor, D. J. Erskine, and C. L. Tang, *J. Opt. Soc. Am. B* **2:** 663 (1985).
46. M. J. Rosker, F. W. Wise, and C. L. Tang, *Appl. Phys. Lett.* **49:** 1726 (1986).
47. M. Ulman, D. W. Bailey, L. H. Acioli, F. G. VallÇe, C. J. Stanton, E. P. Ippen, and J. G. Fujimoto, *Phys. Rev. B* **47:** 10267 (1993).
48. U. D. Keil, D. R. Dykaar, R. F. Kopf, and S. B. Darack, *Appl. Phys. Lett.* **64:** 3257 (1994).
49. T. Elsaessar, J. Shah, L. Rota, and P. Lugli, *Phys. Rev. Lett.* **66:** 1757 (1991).
50. Y. Rosenwaks, M. C. Hanna, D. H. Levi, D. M. Szmyd, R. K. Ahrenkiel, and A. J. Nozik, *Phys. Rev. B* **48:** 14675 (1993).
51. W. S. Pelouch, R. J. Ellingson, P. E. Powers, C. L. Tang, D. M. Szmyd, and A. J. Nozik, *Phys. Rev. B* **45:** 1450 (1992).
52. A. Leitenstorfer, A. Lohner, T. Elsaesser, S. Haas, F. Rossi, T. Kuhn, W. Klein, G. Boehm, G. Traenkle, and G. Weimann, *Phys. Rev. Lett.* **73:** 1687 (1994).
53. M. Koch, D. Weber, J. Feldman, E. O. Göbel. T. Meier, A. Schulze, P. Thomas, S. Schmitt-Rink, and K. Ploog, *Phys. Rev. B* **47:** 1532 (1993).
54. P. C. Becker, H. L. Fragnito, C. H. Brito Cruz, R. L. Fork, J. E. Cunningham, J. E. Henry, and C. V. Shank, *Phys. Rev. Lett.*, **61:** 1647 (1988).
55. K. Leo, M. Wegener, J. Shah, D. S. Chemla. E. O. Göbel, T. C. Damen, and S. Schmitt-Rink, *Phys. Rev. Lett.* **65:** 1340 (1990).
56. K. Leo, E. O. Göbel, T. C. Damen, J. Shah, S. Schmitt-Rink, W. Schäfer, J. F. Müller, K. Köhler, and P. Ganser, *Phys. Rev. B* **44:** 5726 (1991).
57. A. Lohner, K. Rick, P. Leisching, A. Leitenstorfer, T. Elsaesser, T. Kuhn, F. Rossi, and W. Stolz, *Phys. Rev. Lett.* **71:** 77 (1993).
58. M. D. Webb, S. T. Cundiff, and D. G. Steel, *Phys. Rev. Lett.* **66:** 934 (1991).
59. J. Kuhl, E. J. Mayer, G. Smith, R. Eccleston, D. Bennhardt, P. Thomas, K. Bott, and O. Heller, *Semicond. Sci. Technol.* **9:** 429 (1994).
60. D. S. Kim, J. Shah, T. C. Damen, W. Schäfer, F. Jahnke, S. Schmitt-Rink, and K. Köhler, *Phys. Rev. Lett.* **69:** 2725 (1992).
61. W. S. Fann, R. Storz, H. W. K. Tom, and J. Bokor, *Phys. Rev. B* **46:** 13592 (1992).
62. R. Haight, and M. Baeumler, *Surf. Sci.* **287/288** 482 (1993).
63. J. R. Holdman, and J. A. Prybyla, *Phys. Rev. Lett.* **72:** 1364 (1994).
64. C. A. Schmuttenmaer, M. Aeschlimann, H. E. Elsayed-Ali, R. J. D. Miller, D. A. Mantell, J. Cao, and Y. Gao, *Phys. Rev. B* **50:** 8957 (1994).
65. R. Haight, and J. A. Silberman, *Phys. Rev. Lett.* **62:** 815 (1989).
66. J. Bokor, *Science* **246:** 1130 (1989).
67. E. Knoesel, T. Hertel, M. Wolf, and G. Ertl, *Chem. Phys. Lett.* **240:** 409 (1995).
68. C. A. Schmuttenmaer, C. C. Miller, J. W. Herman, J. Cao, D. A. Mantell, Y. Gao, and R. J. D. Miller, *Chem. Phys.* **205:** 91 (1996).
69. K. Hashimoto, M. Hiramoto, T. Kajiwara, and T. Sakata, *J. Phys. Chem.* **92:** 4636 (1988).
70. K. Kemnitz, N. Nakahima, K. Yoshihara, and H. Matsunami, *J. Phys. Chem.* **93:** 6704 (1989).
71. K. Itoh, Y. Chiyokawa, M. Nakao, and K. Honda, *J. Am. Chem. Soc.* **106:** 1620 (1984).
72. Y. Liang, and A. M. Ponte Goncalves, *J. Phys. Chem.* **89:** 3290 (1985).
73. P. V. Kamat, J. P. Chauvet, and R. W. Fessenden, *J. Phys. Chem.* **90:** 1389 (1986).
74. R. W. Fessenden, and P. V. Kamat, *J. Phys. Chem.* **99:** 12902 (1995).
75. F. Willig, R. Eichberger, N. S. Sundrasen, and B. A. Parkinson, *J. Am. Chem. Soc.* **112:** 2702 (1990).
76. B. Trosken, F. Willig, and M. Spitler, *Adv. Materials* **7:** 448 (1995).
77. B. Trosken, F. Willig, and M. Spitler, *J. Phys. Chem.* **99:** 5152 (1995).
78. J. M. Rehm, G. L. McLendon, Y. Nugasawa, K. Yoshihara, J. Moser. and M. Gratzel, *J. Phys. Chem.* **100:** 9577 (1996).
79. J. M. Lanzafame, L. Min, R. J. D. Miller, A. A. Muenter, and B. Parkinson, *Mol. Cryst. Liq. Cryst.* **194:** 287 (1991).
80. J. M. Lanzafame, R. J. D. Miller, A. A. Muenter, and B. A. Parkinson, *J. Phys. Chem.* **96:** 2820 (1992).
81. B. A. Parkinson, *Langmuir.* **4:** 967 (1988).
82. A. Seilmeier, P. O. Scherer, and W. Kaiser, *Chem. Phys. Lett.* **105:** 140 (1984).
83. S. Xu, J. Cao, C. C. Miller, D. A. Mantell, R. J. D. Miller, and Y. Gao, *Phys. Rev. Lett.* **76:** 483 (1996).
84. M. Maroncelli, and G. R. Flemming, *J. Phys. Chem.* **89:** 5044 (1988).
85. M. Maroncelli, *J. Mol. Liq.* **57:** 1 (1993).